Feasibility of a Deep-Space CubeSat Mission with a Stage-Based Electrospray Propulsion System

Feasibility of a Deep-Space CubeSat Mission with a Stage-Based Electrospray Propulsion System

Oliver Jia-Richards and Paulo C. Lozano
Space Propulsion Laboratory
Massachusetts Institute of Technology
Cambridge, MA, 02139
{oliverjr, plozano}@mit.edu

David C. Sternberg, Daniel Grebow, and Swati Mohan
Jet Propulsion Laboratory
California Institute of Technology
Pasadena, CA, 91109
{david.c.sternberg, daniel.grebow, swati.mohan}@jpl.nasa.gov

Abstract*—Independent deep-space exploration with CubeSats, where the spacecraft independently propels itself from Earth orbit to deep-space, is currently not possible due to the lack of high-ΔV propulsion systems compatible with the small form factor. The ion Electrospray Propulsion System (iEPS) under development at the Massachusetts Institute of Technology's Space Propulsion Laboratory is a promising technology due to its inherently small size and high efficiency. However, current electrospray thrusters have demonstrated lifetimes (500 hours) below the required firing time for an electrospray-thruster-propelled CubeSat to escape from Earth starting from geostationary orbit (8000 hours). To bypass this lifetime limitation, a stage-based approach, analogous to launch vehicle staging, is proposed where the propulsion system consists of a series of electrospray thruster arrays and fuel tanks. As each array reaches its lifetime limit, the thrusters and fuel tanks are ejected from the spacecraft exposing a new array to continue the mission. This work addresses the technical feasibility of a spacecraft with a stage-based electrospray propulsion system for a mission from geostationary orbit to near-Earth asteroid 2010 UE51 through a NASA Jet Propulsion Laboratory Team Xc concurrent design center study. Specific goals of the study were to analyze availability of CubeSat power systems that could support the propulsion system and any other avionics as well as requirements for attitude control and communication between the spacecraft and Earth. Two bounding cases, each defined by the maturity of the iEPS thrusters, were considered. The first case used the current demonstrated performance metrics of iEPS on a 12U CubeSat bus while the second case considered expected near-term increases in iEPS performance metrics on a 6U CubeSat bus. A high-level overview of the main subsystems of the CubeSat design options is presented, with a particular focus on the propulsion, power, attitude control, and communication systems, as they are the primary drivers for enabling the stage-based iEPS CubeSat architecture.

TABLE OF CONTENTS

1. INTRODUCTION

The exploration of small asteroids through the use of miniature spacecraft such as CubeSats could provide substantial benefits in terms of affordability, visit rates, and overall science return. CubeSats have demonstrated considerable capabilities with examples such as the AeroCube program [1], the Radar in a CubeSat (RainCube) technology demonstration mission for Ka-band precipitation radar technologies [2], and the Arcsecond Space Telescope Enabling Research in Astrophysics (ASTERIA) mission which demonstrated the capability for a CubeSat to detect transiting exoplanets [3]. However, all of these missions were limited to low-Earth orbit due in part to the lack of high ΔV propulsion systems compatible with the CubeSat form factor. To date, only the Mars Cube One (MarCO) CubeSats [4] have left Earth orbit and demonstrated many of the subsystems required for a deep-space mission. These CubeSats shared a ride with the InSight lander and the propulsion system [5] was only capable of $\sim$40 m/s of ΔV and was intended only for attitude control and trajectory correction maneuvers [6].

One of the remaining technology gaps required to open up deep-space missions to CubeSats is the development of high ΔV propulsion systems that are compatible with the small form factor. Many CubeSat propulsion systems have been proposed and developed [7], [8], [9]. However, due to difficulties with the miniaturization of propulsion systems such that they are compatible with the CubeSat form factor, very few CubeSat propulsion systems have flight heritage. The majority of those that do are cold gas systems [7] which cannot be used for high ΔV missions due to their low ($\sim$80 s) specific impulse. Electrospray thrusters are a promising technology for CubeSat propulsion due to their inherent flexibility in scaling [9]. However, their ΔV output is currently limited by the operational lifetime of the thrusters [10]. For a deep-space mission starting in geostationary orbit, the required ΔV for escape is approximately 2.66 km/s when low-thrust losses have been accounted for. For a 15 kg, 6U CubeSat with an electrospray-thruster-based propulsion system, approximately 8000 hours of constant firing time are required to achieve the given ΔV. Current electrospray thrusters have lifetimes of around 500 hours, which is insufficient to perform such a mission. Even if trajectories which attempt to minimize the required firing time are devised or if expected near-term advancements in electrospray thruster performance are met, the firing time of an individual thruster will be lower than the required firing time for escape [11].

To bypass the lifetime limitation of an individual thruster, a stage-based approach, analogous to launch vehicle staging, is proposed. The propulsion system consists of a sequence of electrospray thruster arrays each with their own thrusters and fuel tanks. As each array reaches its lifetime limit or shows signs of significant performance degradation, it is ejected

from the spacecraft exposing a new array to continue the mission. Such an approach is normally not feasible with other types of propulsion devices as it significantly increases the total mass and volume of the propulsion system. However, the inherent low mass and size of electrospray thrusters allows multiple stages to be added without exceeding the mass and volume constraints of the spacecraft bus [12]. In effect, the overall performance of the propulsion system is increased without relying on developments in the underlying propulsion technology.

Staging of electrospray thrusters was originally analyzed in [13] to explore reductions in the transfer time of a lunar mission. Preliminary design and analysis on the required mechanisms for a stage-based approach are investigated in [11] along with analysis of the use of staging for missions to several near-Earth asteroids. Most recently, a laboratory demonstration of staging with electrospray thrusters was conducted in [14] which demonstrated the mechanical and electrical feasibility of such a configuration. This work contributes towards the development of staging systems for electrospray thrusters by investigating the technical feasibility of integrating such a propulsion system into a CubeSat in order to enable deep-space missions. A high level overview of the different subsystems is presented to assess the mission's feasibility with a more detailed analysis of the propulsion, power, attitude control, and communication systems, as they are the primary drivers for enabling the stage-based iEPS CubeSat architecture.

2. System Overview

The goal of this work was to determine whether or not a CubeSat mission to a near-Earth asteroid with a stage-based electrospray propulsion system is possible with current or near-term technology. The spacecraft is to start from geostationary orbit and independently propel itself into deep-space and to the asteroid. The desired form factor is a 6U CubeSat but is allowed to increase to 12U if necessary. The mission goal is primarily a technology demonstration of the propulsion system but includes limited science focused around visual surveys of the asteroid. As such, mission success would be determined if the spacecraft rendezvous with the asteroid and not through any science objectives. If such a mission were successful, the capabilities of CubeSats would be dramatically increased - missions to asteroids or other planets would be possible without requiring a rideshare with a primary payload headed to the same destination. In addition, the use of standardized and miniature spacecraft for exploration of asteroids has the potential to dramatically decrease the cost of science over the current paradigm of a single monolithic spacecraft.

The MarCO spacecraft was used as the starting point for the overall system design as it provides deep-space flight heritage for many of the subsystems. The primary change from the MarCO design is the use of the stage-based electrospray propulsion system in place of the cold gas system that MarCO used. The change to an electric propulsion system drives many of the other changes including any necessary changes to spacecraft configuration and increased power requirements. As a result, the required solar panels are larger and need gimbals in order to decouple pointing of the spacecraft for long-duration maneuvers and pointing of the solar panels towards the Sun. Figure 1 shows a notional diagram of the spacecraft internal configuration for the desired 6U form factor. In the diagram, the solar panels extended into and out of the page. The primary goal of the study was to ensure that the change in propulsion system and subsequent increase in solar array size did not make the mission infeasible.

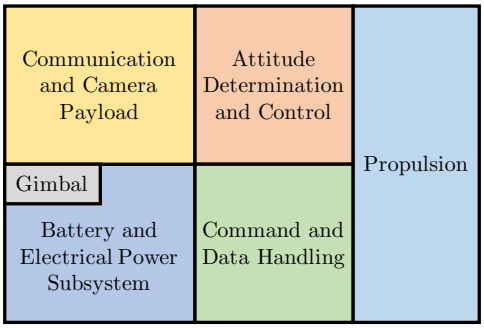

Figure 1. Notional spacecraft internal configuration

The choice of mission also results in changes to the system architecture. Since the mission target is a near-Earth asteroid as opposed to Mars, the requirements on the communications system are relaxed. As such, only the wide beam patch antennas are required and the high-gain reflectarray, ultra-high frequency antenna, and medium-gain antenna can be removed from the system opening up more mass and volume for the increased solar array size and any thermal management. In addition, as the mission was considered to be a technology demonstration, the only payload is the camera that was also used on MarCO. Other changes to the overall system include upgrades to the command and data handling system as well as an upgrade to the Iris transceiver [15].

3. Propulsion

Electrospray thrusters produce thrust through electrostatic acceleration of ions. Ions are evaporated from an ionic liquid propellant, typically EMI-BF_4, by overcoming the surface tension of the liquid with an applied electric field. The ionic liquid propellant is a molten salt at room temperature that is non-reactive, readily available, and has low toxicity. Electrospray thrusters and their ionic liquid propellants hold three main advantages that make them an excellent choice for propulsion of small spacecraft such as CubeSats. Firstly, the ionic liquid is "pre-ionized" and does not need an ionization chamber. Second, ionic liquids have near-zero vapor pressure due to the ionic bonds between molecules and therefore do not need any form of pressurized containment [16]. Lastly, the propellant is fed to the thruster by passive capillary forces through a porous liner embedded into the fuel tank thereby eliminating the need for any propellant management systems. These three advantages allow electrospray thrusters to be incredibly compact and suitable for the CubeSat form factor.

To produce a strong enough electric field to evaporate the ions, the ionic liquid is fed to a sharp emitter tip. A potential is applied to the ionic liquid with respect to an extractor grid. The sharp tip of the emitter allows for a strong electric field to develop that causes a liquid instability and the development of a sharp liquid meniscus that accentuates the electric field to the point that ions can be evaporated from the liquid [17]. A diagram of a single emitter and extractor grid is shown in Figure 2. The thrust produced by a single emitter-extractor pair is only on the order of 10s of nano-Newtons. Therefore, multiple emitters are arranged in an array to produce a single thruster. Since a single emitter is on the 100 μm scale, arrays of 100s of emitters can be manufactured on the 1 cm scale.

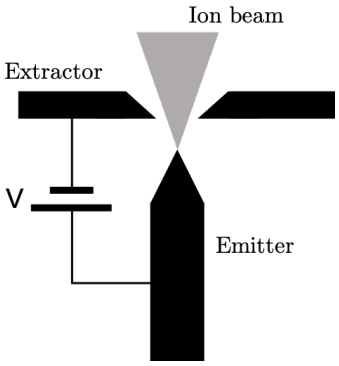

Figure 2. Diagram of single emitter and extractor grid

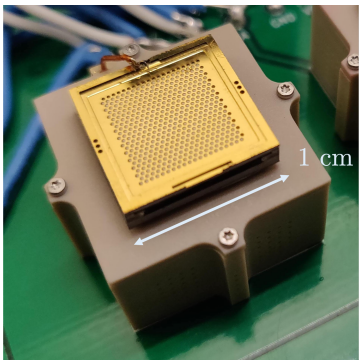

Figure 3. iEPS thruster mounted on single thruster fuel tank

This study considers the ion Electrospray Propulsion System (iEPS) under development in the Space Propulsion Laboratory (SPL) at the Massachusetts Institute of Technology. Each iEPS thruster consists of an array of 480 emitter tips made from porous glass. The emitter array is housed in a 13 x 12 x 2.4 mm silicon frame with a gold coated silicon extractor grid. Figure 3 shows an iEPS thruster mounted on a single thruster fuel tank. Due to the passive propellant feed system, the same iEPS thruster can be mounted on a variety of fuel tanks as long as a porous material connection exists between the ionic liquid and emitter array. Figure 4 shows a scaled-up configuration where four iEPS thrusters are mounted on the same fuel tank, maximizing the density of emitter tips while maintaining structural integrity during launch from Earth.

Each iEPS thruster can produce thrust in the range of 2 - 20 μN with a specific impulse close to 1000 s when using EMI-BF_4 as the ionic liquid propellant [10]. However, the thrust and specific impulse are heavily dependent on the ionic liquid

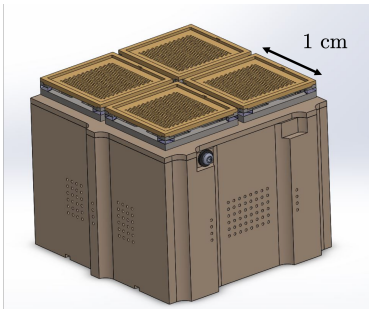

Figure 4. Four iEPS thrusters mounted on a cluster fuel tank

Table 1. Performance regimes of iEPS thrusters

	Minimum	Target
Max thrust	20 μN	80 μN
Specific impulse	1000 s	2500 s
Power	0.16 W	1.25 W
Lifetime	500 hr	1000 hr

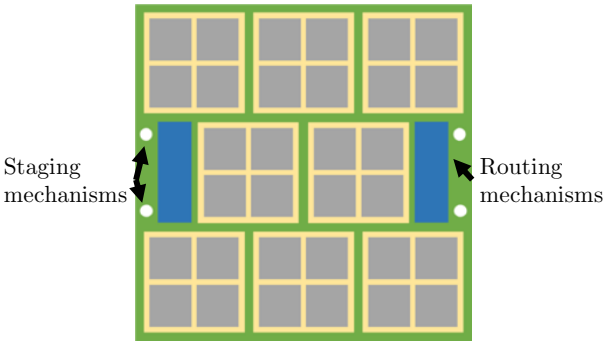

Figure 5. iEPS thruster configuration on a 1U CubeSat face

used as well as the material of the emitter array. Ongoing research at the SPL is investigating different materials for the emitter array that can contribute to an increased thrust, specific impulse, and thruster lifetime [18]. Two regimes of thruster performance are considered throughout this work. The first represents the current demonstrated performance which is the minimum expected performance of the thrusters during implementation. The second represents the target performance which is based on expected near-term developments. The performance metrics for a single thruster in both the minimum and target performance regimes are summarized in Table 1.

A single iEPS thruster on its own does not produce enough thrust to be useful for main propulsion of a CubeSat mission. While the low thrust has other applications, such as for high precision attitude control [19], for main propulsion the thrust is increased by using arrays of thrusters. Tanks with four thrusters each, as shown in Figure 4, are arranged on a 1U CubeSat face. A 1U CubeSat face can hold up to nine of these clusters in a 3 x 3 square pattern for a total of 36 thrusters. For this work, we will consider a configuration where a thruster in the center row is omitted to provide space for mechanisms required for the staging system on either side of the thrusters as shown in Figure 5. Two mechanisms are required for the staging system: a staging mechanism that connects successive stages and ejects the outermost stage at the time of staging, and a routing mechanism that passively routes thruster control signals from the power processing unit to the active stage. As the signal routing is done mechanically and passively, the power processing unit is "stage blind" and does not track which stage is active. This allows the same power processing unit to be used for a staged configuration as well as a traditional single array configuration. Further information on the staging and routing mechanisms can be found in [11] and [14]. This configuration, while designed for a 3U CubeSat, is easily scalable to large form factors. For a 6U CubeSat, two thruster boards are placed side by side on one of the spacecraft's 20 cm x 10 cm faces while for a 12U CubeSat, four thruster boards are placed in a square pattern on one of the spacecraft's 20 cm x 20 cm faces.

The primary ΔV limitation of electrospray thrusters is their

operational lifetime. Models as well as experimental techniques to analyze various lifetime limitations are developed in [20] and [21]. For iEPS thrusters, the two main life-limiting mechanisms are propellant accumulation on the extractor grid as well as arcing between isolated tips on the emitter array and the extractor grid. The beam of ions which is extracted from an emitter tip leaves in a conical shape with observed half angles of up to 60 degrees [10]. The beam can therefore impact the extractor grid and allow propellant to accumulate or backspray onto the emitter array. If enough propellant accumulates, an ionic liquid connection can form between the emitter array and extractor grid causing an electrical short on the thruster and rendering it inoperable. In addition, not all tips on the emitter array will be identical due to difficulties with repeatable manufacturing and inherent material non-uniformity [18]. While most emitter tips will operate as intended, some emitter tips might have unstable menisci [17] which can lead to erratic liquid emission and occasional electrical discharges between the emitter tip and extractor grid [22] degrading the thruster's performance over time.

A stage-based approach allows these lifetime limitations to be bypassed in order to increase the overall lifetime of the propulsion system. While improvements could be made towards the lifetime of individual thrusters through a better understanding and mitigation of the life-limiting mechanisms, the use of staging is a strategy that could enable high ΔV capabilities with existing electrospray technology. Furthermore, the use of staging systems in deep-space missions would provide additional redundancy and reliability, even for thrusters with improved lifetime, as fresh thruster arrays could replace functioning, albeit degraded, ones.

The drawback of using a stage-based approach is that it increases the mass and volume of the propulsion system over that of a conventional, "single-stage" system. Analytical methodologies for determining the required number of stages for a given mission, which sets the overall propulsion system mass and volume, are developed in [23]. For a mission, defined by its ΔV, the required number of stages, N, is

$$N = \frac{m_0 + \frac{1}{2}m_\mathrm{d}}{\frac{1}{2}m_\mathrm{d} + \frac{FL}{\Delta \mathrm{V}} + \frac{1}{2}\frac{FL}{c}} \tag{1}$$

where m_0 is the initial wet mass of the spacecraft, m_d is the dry mass of an individual stage, F is the propulsion system thrust, L is the lifetime of an individual thruster, and c is the ideal exhaust velocity. The dry mass of an individual stage can be calculated as

$$m_\mathrm{d} = m_\mathrm{s} + m_\mathrm{h} + \gamma\frac{FL}{c} \tag{2}$$

where m_s is the mass of the staging electronics, m_h is the mass of the thruster heads as well as the board the thrusters are mounted on, and γ is the structure-to-fuel mass ratio for the fuel tanks. The mass of the stage-based propulsion system, m_staged, can then be calculated as

$$m_\mathrm{staged} = N(1+\gamma)\frac{FL}{c} + \mathtt{ceil}(N)(m_\mathrm{s} + m_\mathrm{h}) + m_\mathrm{PPU} \tag{3}$$

where m_PPU is the mass of the power processing unit. For comparison, the mass of an unstaged propulsion system, m_unstaged, can be calculated as

$$m_\mathrm{unstaged} = m_0(1+\gamma)\left(1 - e^{-\Delta \mathrm{V}/c}\right) + m_\mathrm{h} + m_\mathrm{PPU} \tag{4}$$

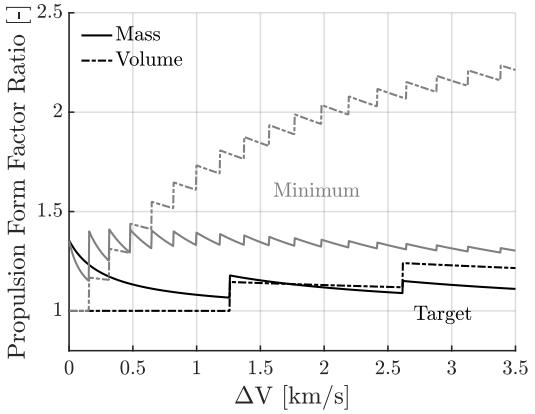

Figure 6. Ratio of staged to unstaged mass and volume

For the volume, the base area of the thrusters is fixed based on the configuration shown in Figure 5. Therefore, as stages are added or the fuel per stage is increased, only the height of the system changes. The height of the stage-based propulsion system, h_staged, can be calculated as

$$h_\mathrm{staged} = \frac{N}{\rho M A}\frac{FL}{c} + \mathtt{ceil}(N)h_\mathrm{s} + h_\mathrm{PPU} \tag{5}$$

where ρ is the fuel density, M is the number of thrusters per stage, A is the cross-sectional area of the tank allotted for fuel, and h_s accounts for the height of the stage board, the caps on the fuel tanks, and the thruster head. The height of an unstaged propulsion system, h_unstaged, can be calculated as

$$h_\mathrm{unstaged} = \frac{m_0}{\rho M A}\left(1 - e^{-\Delta \mathrm{V}/c}\right) + h_\mathrm{s} + h_\mathrm{PPU} \tag{6}$$

Figure 6 shows the ratio of staged to unstaged propulsion system mass and volume at various ΔV requirements for performance parameters given in Table 2 which is representative of both the minimum and target iEPS performance cases. The discrete jumps are caused by transitions between integer values of the required number of stages and the `ceil` function in the staged system's mass and height.

In the minimum performance case, there is a fairly constant 30% increase in system mass and a continuously increasing volume penalty that reaches 120% at 3.5 km/s of ΔV. A system capable of producing 3.5 km/s of ΔV is 7.43 kg and occupies 3.9U requiring either a reduction in the volume of other subsystems or increasing the CubeSat bus to 12U. If a "single-stage" system could be produced, it would occupy only 1.8U, similar to the volume of the MarCO propulsion system, and would be compatible with a 6U form factor.

In the target case, we can see that there is also a fairly constant increase in system mass, this time at 12.5%, and a continuously increasing volume penalty that reaches 21.6% at 3.5 km/s. In this case, a system capable of producing 3.5 km/s of ΔV is 2.94 kg and occupies 1.5U - compatible with a 6U form factor. For comparison, this system is 16% lighter and occupies 15% less volume than the MarCO propulsion system yet produces 8,650% more ΔV.

Table 2. Parameters for propulsion system mass and volume

Parameter	Minimum	Target
Spacecraft wet mass	15 kg	15 kg
Staging mechanism mass	75 g	75 g
Thruster and board mass (m_{h})	53 g	53 g
Stage height (h_{s})	70 mm	70 mm
PPU mass	0.16 kg	0.16 kg
PPU height	3 cm	3 cm
Thrust	1.28 mN	5.12 mN
Lifetime	500 hr	1000 hr
Specific impulse	1000 s	2500 s
Structural mass ratio	0.22	0.22
Fuel mass density	1.5 g/cc	1.5 g/cc
Tank base area	9 cm^2	9 cm^2

4. POWER

The power system consists of the electrical power subsystem (EPS) electronics, the solar panels, and the battery. In both cases, the spacecraft-Sun distance is approximately 1 AU throughout the escape spiral away from Earth and rendezvous with 2010 UE51. Despite the relatively constant mission profile, the difference in system architectures greatly impacts the power subsystem. In the minimum performance case, 10 W of power are required to operate the thrusters during firing while in the target performance case, 80 W are required.

Throughout the mission it is assumed that the thruster is on except during and shortly after eclipses, in order to allow for battery recharge. For both system architectures, the maximum eclipse duration is approximately 85 minutes. It is also assumed that communications with Earth are limited to 1 hour at a time throughout which the thrusters are left on and the spacecraft is not required to be power positive. The goal of the power system is to size the solar panels and battery in order to provide sufficient power throughout operations with a 15% contingency on all loads. Additional goals are to minimize the battery recharge duration after eclipses and the solar array size.

For both system architectures the MarCO EPS built by AstroDev is assumed. This decision relies on the capability of the MarCO EPS to be able to handle 140 W of power processing required for the target performance system architecture. Throughout MarCO operations the maximum solar array production was approximately 35 W [4] and the max power capability of the MarCO EPS is unknown. However, in the case that the MarCO EPS is unable to support the required power, the Gomspace P60 EPS is an alternative option that should be able to meet the mission needs.

Panasonic NCR-18650B cells are used for the battery. These are the same cells as used on MarCO but in a different configuration in order to provide sufficient voltage to operate the thruster power processing unit. A total of 12 cells are used with three parallel strings each composed of four cells in series. Assuming that each cell has 2.2 Ah of capacity, the total beginning-of-mission energy capacity of the battery is 83 Wh. The battery capacity is sufficient to power the spacecraft during eclipse in both system architectures as the thrusters are turned off during eclipse.

For the minimum thruster performance system architecture, an eight panel HAWK solar array from MMA with triple-junction (ZTJ) solar cells is used. The solar array is split into two wings with four panels each. Each panel holds seven 26.62 cm^2 cells for a total active area of 0.149 m^2 providing an expected beginning-of-mission power of 57 W and expected end-of-mission power of 47 W. Each wing requires a single-axis gimbal in order to stay sun-pointed during the escape spiral away from Earth.

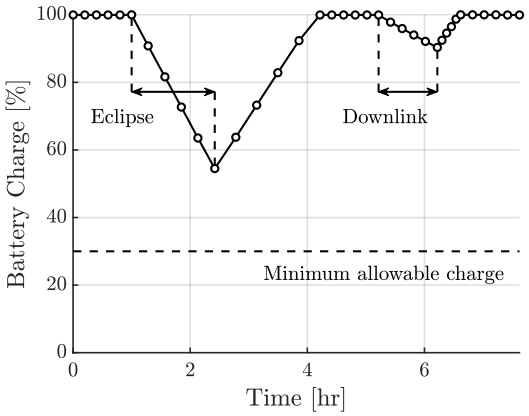

Figure 7. Battery charge during operations for minimum thruster performance system architecture

Figure 7 shows the battery charge during expected operations. Two cases are considered: eclipse followed by battery recharge and communications while thrusting. The minimum battery charge of 55% occurs at the end of the eclipse and is above the minimum allowable charge of 30%. We can also see that during downlink the spacecraft is not power positive, but the batteries provide sufficient energy storage to supplement the solar arrays and allow the thrusters to continue to fire while the spacecraft is communicating.

For the target thruster performance system architecture, a six panel solar array with ZTJ cells from Blue Canyon Technologies (BCT) is used. The solar array assumes that two additional panels can be added to the 6U-V Double Wing Solar Array currently offered by BCT. The solar array is split into two wings with three panels each. Each panel holds 24 26.62 cm^2 panels for a total active active area of 0.383 m^2 providing an expected beginning-of-mission power of 146 W and expected end-of-mission power of 121 W. As in the minimum thruster performance architecture, each wing requires a single-axis gimbal in order to stay sun-pointed during the escape spiral.

Figure 8 shows the battery charge during expected operations. As before, two cases are considered: eclipse followed by battery recharge and communications while thrusting. The minimum battery charge of 46% occurs at the end of eclipse and is above the minimum allowable charge of 30%. Again, the spacecraft is not power positive during downlink but the batteries provide sufficient energy storage to supplement the solar arrays and allow the thrusters to continue to fire while the spacecraft is communicating.

The primary risks with the power system occur in the target thrust performance architecture. The first risk is that the MarCO EPS might not be able to process the max (146 W) power from the solar arrays. However, the Gomspace P60 is a high-power EPS for small satellites that should be able to meet the mission needs. The second risk is the assumption that two panels can be added to the 6U-V Double Wing Solar Array from BCT. While BCT does offer a lower-power (118

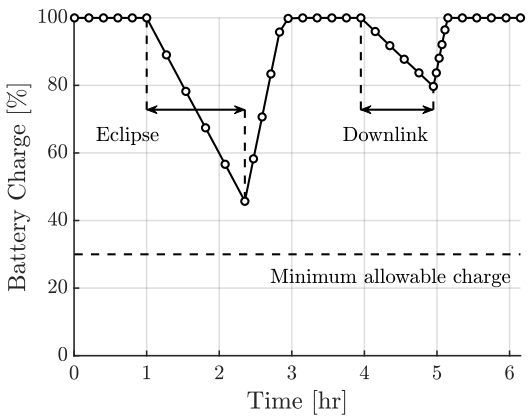

Figure 8. Battery charge during operations for target thruster performance system architecture

W) 6U-H Triple Wing Solar Array with six panels, there is no guarantee that the two panel extension for the 6U-V can be deployed and stowed on a 6U CubeSat.

In the case that the power requirements for the target thruster performance cannot be met, an alternative option is to reduce the thruster power such that the 6U-H Triple Wing Solar Array can be used. This option would slightly increase the mission time and required fuel mass but reduce the required power to within the capabilities of currently offered commercial-off-the-shelf solar arrays.

5. MISSION DESIGN

Asteroid 2010 UE51 passes within 0.025 AU of Earth in December 2023. Because the Earth-relative speed of the asteroid at closest approach is relatively low, approximately 1.3 km/s, a CubeSat low-thrust mission to the asteroid is feasible during this time. The cost of the mission is reduced by assuming the spacecraft rideshares with another mission to geostationary orbit, where the CubeSat is deployed. The spacecraft then thrusts, spiraling out from geostationary orbit, eventually escaping Earth orbit and rendezvousing with 2010 UE51. For the purposes of this analysis, "rendezvous" is defined as the spacecraft matching the heliocentric position and velocity of 2010 UE51.

Missions were examined to 2010 UE51 for both the minimum and target thruster performance cases. A summary of the missions is provided in Table 3. The transfers are optimized with JPL's high-fidelity low-thrust optimization software Mystic [24], [25], assuming a full ephemeris solar system point-mass gravitational model including the Moon. Deployment from geostationary orbit and rendezvous times are optimized. The overall objective is to minimize time of flight. For both trajectory designs it is assumed that the spacecraft thrusts continuously, even while uplinking or downlinking data, or while passing through eclipse. The trajectories are locally optimal point solutions. Several other solutions exist that require less propellant.

For the minimum performance case, the CubeSat is deployed from geostationary orbit on December 15, 2022, and arrives at 2010 UE51 on January 22, 2024. During the transfer there are 0.1 kg mass drops every 500 hours to model the ejection of each thruster stage. Twenty stages are required for the mission. A plot of the trajectory for the minimum performance case is shown in Figure 9. The total time of flight for the mission is 403 days and the spacecraft mass at rendezvous is 8.65 kg.

Table 3. 2010 UE51 mission design summary

	Minimum	Target
Depart GEO	Dec 15, 2022	Sep 5, 2023
Earth revs	98	25
Earth escape	Nov 16, 2023	Dec 19, 2023
Rendezvous	Jan 22, 2024	Feb 9, 2024
Time of flight	403 days	157 days
Number of stages	20	4
Rendezvous mass	8.65 kg	11.87 kg
Propellant mass	4.45 kg	2.83 kg
ΔV	3.76 km/s	5.18 km/s
Max Earth range	0.033 AU	0.049 AU
Solar range	0.98-1.02 AU	0.99-1.02 AU
Total shadow time	15.6 hr	22.4 hr
Max shadow transit	95 min	89 min

For the target case, the spacecraft departs geostationary orbit on September 5, 2023, and rendezvous with 2010 UE51 on February 9, 2024. There are 0.1 kg mass drops every 1000 hours for each depleted stage, and only four stages are required for the mission. A plot of the trajectory is shown in Figure 9. The time of flight is 157 days and the rendezvous mass is 11.87 kg. While the ΔV requirement is higher for the target performance case, this is primarily driven by the choice of optimizing for minimum time of flight. If the optimization was modified to minimize ΔV, then the expected ΔV of the mission would be closer to 3.5 km/s.

As expected, since 2010 UE51 is a near-Earth asteroid with a relatively low Earth-relative close approach speed, the spacecraft always remains within 0.05 AU of Earth and therefore the heliocentric range is close to 1 AU. Because the spiral out from geostationary orbit is primarily Earth-equatorial (out of the ecliptic), the total time in shadow is a small fraction of the transfer, less than 1%.

6. COMMUNICATION

The requirements on the communication system are for basic telemetry during escape and cruise and sufficient data volume to transmit pictures after rendezvousing with asteroid 2010 UE51. In addition a bit error rate of 10^{-5} is required. It is assumed that a 34-meter antenna from the Deep Space Network (DSN) is used for both uplink from and downlink to Earth. All communications occur in X-Band frequencies at 8.4 GHz for uplink and 7.1 GHz for downlink.

The communication system uses an Iris v2.1 transceiver [15] with a solid-state power amplifier and low noise amplifier. In both cases the spacecraft stays relatively close to Earth with maximum spacecraft-Earth distances of 0.05 AU in the minimum thruster performance case and 0.03 AU in the target thruster performance case. Therefore, the only antennas on the spacecraft are low-gain patch antennas. A total of four antennas are used with two pairs of receive and transmit antennas placed on opposite sides of the spacecraft allowing for near-omnidirectional antenna field-of-view. Figure 10 shows a notional diagram of the antenna locations on the spacecraft bus as well as their fields of view. Both the Iris transceiver and

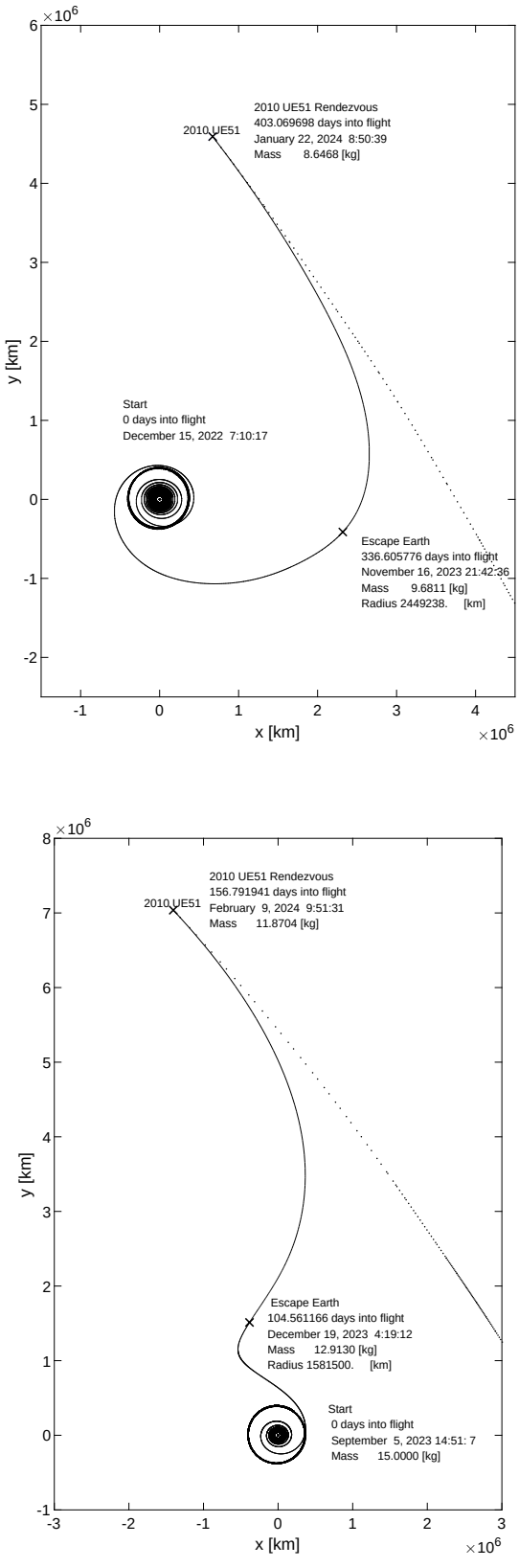

Figure 9. Earth-centered inertial plot of trajectory for minimum (top) and target (bottom) performance

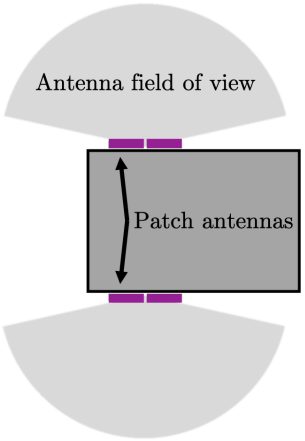

Figure 10. Notional antenna locations and fields of view

low-gain patch antennas have demonstrated flight heritage on a deep-space CubeSat from the MarCO mission [26]. The communication system is identical between the two system architectures due to their similar trajectories.

The proposed communication system allows for at least 4 kb/s downlink and 1 kb/s uplink in both system architectures which will be processed by the command and data handling subsystem. The command and data handling system uses a JPL-built Sphinx system designed for deep-space missions. The Sphinx system consists of two cards, each compatible with the CubeSat form factor, and allows for 1 kb/s uplink and 4 kb/s downlink, consistent with the communication system. The command and data handling system is also identical between the two system architectures.

7. Attitude Control

The attitude control system is tasked with pointing the spacecraft for several tasks including: orienting the thrusters along the commanded thrust axis, pointing the solar panels towards the sun, and pointing the antenna boresight towards Earth ground stations. The selected design leverages a Blue Canyon Technologies XACT-15 unit which has demonstrated flight heritage for use on a deep-space CubeSat from the MarCO mission [26]. The MarCO pointing performance was sufficiently tight to meet the projected pointing requirements of $\pm 2^\circ$ for thruster pointing, $\pm 5^\circ$ for solar array pointing, and $\pm 1^\circ$ for antenna pointing [6]. The attitude control system design is the same for both of the system architectures considered in the study.

Figure 11 shows an example XACT-15 unit. The XACT-15 contains three P015 reaction wheels, each with 15 mNms of momentum storage capability and a maximum torque of 4 mNm. The reaction wheels are mounted orthogonal to each other on isolators for vibration damping. The XACT-15 also contains an inertial measurement unit (IMU) for high frequency attitude rate sensing and a stellar reference unit (SRU) for precise attitude determination. For sun search maneuvers during safe mode and initial deployment, a pair of coarse sun sensors, each with four diodes, provide the direction of the sun with respect to the spacecraft. The sun sensors are mounted externally from the XACT-15 unit such that they can be mounted on different faces of the bus.

The SRU provides the highest accuracy attitude knowledge

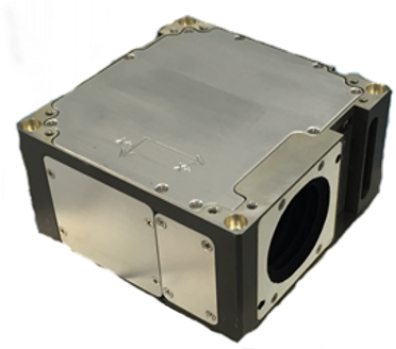

Figure 11. Blue Canyon Technologies XACT-15

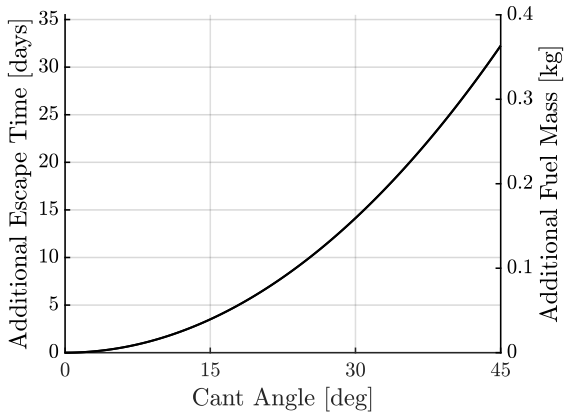

Figure 12. Additional time and fuel mass required to escape due to canting thrusters

though it can only operate at low rotation rates. For higher rotation rates, the SRU is unable to track the motion of the star field and the spacecraft attitude is propagated using the IMU. To maintain the best performance from the SRU, spacecraft operations are designed to prevent the sun or lit portion of the Earth from entering keep-out zones, areas within which stray light would detract from the attitude estimate accuracy.

As the reaction wheels operate for extended periods of time, they slowly acquire angular momentum to maintain fixed body pointing as a result of external disturbance torques such as solar radiation pressure and gravity gradients. The reaction wheels are therefore periodically desaturated by creating torques about each of the spacecraft body axes with the propulsion system. In the configuration shown in Figure 5, the distributed array of electrospray thrusters allows for torques to be created about two of the body axes. Two options exist for creating a torque about the third body axis: cant some of the thrusters inward, similar to how the MarCO thrusters were canted, or add additional thrusters not on the stages that are dedicated to performing desaturations.

Both options require minor modifications to the current thruster configurations. Canting thrusters will require modifying some of the thruster tanks to allow the thruster heads to be canted while adding additional thrusters will require modification to the power processing unit to control the thrusters as well as for thruster mounting as these thrusters would not be placed on the individual stages. Both options also reduce the available payload mass. Adding additional thrusters directly impacts the payload mass through the mass of the additional thrusters. Canting thrusters indirectly impacts the payload mass as it reduces the axial thrust of the propulsion system. The reduced axial thrust both increases the firing time required to achieve escape and increases the low-thrust losses during the escape trajectory. Figure 12 shows the additional time and fuel mass required to escape due to canting four of the thruster clusters on each stage. For reference, the MarCO attitude control thrusters were canted by 30 degrees [6]. We can see that the additional fuel mass required is modest (100-300 g) and approximately the same mass that would be required to add additional thrusters. Both canting thrusters and adding additional thrusters are feasible options. More detailed analysis is required to determine which option would be better for this mission.

In order to orient itself, the XACT-15 unit requires onboard knowledge of the spacecraft's position along its trajectory. The trajectory can be modeled with a set of Chebyshev polynomials in a manner similar to that used by MarCO and what will be used by Lunar Flashlight [6], [27]. To support regular onboard ephemeris updates from the ground, JPL developed ground-based tools to convert MarCO trajectories into Chebyshev polynomial coefficients that could be uploaded to the spacecraft and stored within the XACT-15 unit's memory. A similar process can be used in this for both system architectures: the desired trajectory is modeled as a set of eight Chebyshev polynomial coefficients per axis, thereby requiring a small data product to be uplinked to adjust the onboard ephemeris as additional ground-based position estimates are generated.

There are several risks that face the attitude control system. First, there is a risk that flexible modes from the large, hinged solar arrays could require an extended controller tuning process. Blue Canyon Technologies worked closely with MarCO to develop the attitude controllers, so it is expected that a similar process will be followed for this mission. Additionally, there is a risk that the attitude control system components will not survive for extended times beyond the low-Earth orbit environment. The deep-space radiation environment can lead to single event upsets and disrupt nominal spacecraft operations. Therefore, further radiation testing and analysis may be necessary, possibly leading to the use of radiation shielding around more sensitive components. Another risk is that the thrusters conducting the reaction wheel desaturations may require extended periods of firing to counter angular momentum changes during staging events, which have yet to be fully analyzed. Therefore, it is expected that the separation mechanism will be designed for low-torque actuation.

8. THERMAL

The thermal system is required to maintain the bus electronics between -20 °C and 50 °C. It is assumed that peak power dissipation while in the near-Earth environment is 67 W and the minimum power dissipation for survival in deep-space is 20 W for both system architectures. In addition, in both cases the spacecraft-Sun distance varies between 0.98 AU and 1.07 AU and the propulsion system power processing unit has an efficiency of approximately 80%.

In the minimum thruster performance case, the required radiator area is approximately 850 cm^2 which would use 27% of the surface area of a 12U CubeSat bus. For survival, 16.4 W of heat dissipation is required to maintain the minimum allowable temperature. As the minimum spacecraft bus

dissipation is 20 W, no additional heaters are required but replacement heaters will be carried for redundancy.

In the target thruster performance case, the required radiator area is approximately 1300 cm^2 which would use 59% of the surface area of a 6U CubeSat bus. For survival, 25.4 W of heat dissipation is required. Since the minimum spacecraft bus dissipation is 20 W, additional heaters are required in order to maintain the minimum allowable temperature.

9. Conclusion

A preliminary assessment has shown that a deep-space CubeSat mission with a stage-based electrospray propulsion system is feasible in the near future. The MarCO spacecraft was used at a starting point for the design to leverage its flight heritage with modifications made for the different propulsion system and trajectory. The primary concerns with the architecture are in the propulsion system, due to its novelty, and the power system, due to the high power requirements of the electrospray thrusters. There are no major concerns with the communication system. However, this is aided by the choice of target asteroid which keeps the spacecraft relatively close to Earth (< 0.05 AU).

Developments in the ion Electrospray Propulsion System [28] continue to be made in parallel to developments in the stage-based propulsion system. The mechanical and electrical feasibility of the stage-based propulsion system has already been demonstrated [14]. Future work in the Space Propulsion Laboratory aim to perform environmental testing of the staging system in the configuration shown in Figure 5 as well as characterizing the expected performance of the thrusters in order to move towards a flight-ready system. In addition, work at the NASA Jet Propulsion Laboratory is analyzing different thruster configurations and the use of the stage-based electrospray propulsion system for trajectory and attitude control as well as momentum management.

In terms of power system, the design cases considered for this study were assumed to bound the performance metrics of the propulsion system. In the highest-power case, the required power is beyond currently offered commercial-off-the-shelf solar arrays. However, the highest power requirement, downlink and thruster firing, is only 13% higher than the currently offered 6U-H Triple Wing Solar Array from Blue Canyon Technologies. An alternative option is to reduce the thruster power. With the target thrust performance metrics, the propulsion system is already smaller and lighter than the MarCO cold gas thruster system. Reducing the thruster power would trade the extra mass and volume in order to potentially reduce the overall spacecraft power consumption to within currently offered solar arrays.

Acknowledgments

Funding for this work was provided by the NASA Space Technology Mission Directorate through the Small Spacecraft Technology Program under grant 80NSSC18M0045 and through a NASA Space Technology Research Fellowship under grant 80NSSC18K1186. Parts of this work were carried out at the Jet Propulsion Laboratory, California Institute of Technology, under a contract with the National Aeronautics and Space Administration (80NM0018D0004). In addition, P. C. Lozano would like to thank the Miguel Alemán-Velasco foundation for its support.

References

[1] D. Hinkley and B. Hardy, "Picosatellites and Nanosatellites at The Aerospace Corporation," in *In-Space Non-Destructive Inspection Technology Workshop*, Johnson Space Center, Houston, TX, February-March 2012.

[2] E. Peral *et al.*, "RainCube, a Ka-band Precipitation Radar in a 6U CubeSat," in *Proceedings of the 31st Annual AIAA/USU Conference on Small Satellites*.

[3] M. W. Smith *et al.*, "On-Orbit Results and Lessons Learned from the ASTERIA Space Telescope Mission," in *Proceedings of the 32nd Annual AIAA/USU Conference on Small Satellites*, Logan, UT, August 2018.

[4] A. Klesh and J. Krajewski, "MarCO: CubeSats to Mars in 2016," in *Proceedings of the 29th Annual AIAA/USU Conference on Small Satellites*, Logan, UT, August 2015.

[5] VACCO Industries. JPL MarCO - Micro CubeSat Propulsion System. [Online]. Available: https://www.cubesat-propulsion.com/wp-content/uploads/2015/11/JPL-MarCO-Micro-CubeSat-Propulsion-System-datasheet.pdf

[6] D. Sternberg, J. Essmiller, C. Colley, A. Klesh, and J. Krajewski, "Attitude Control System for the Mars Cube One Spacecraft," in *Proceedings of the 40th IEEE Aerospace Conference*, Big Sky, MT, March 2019.

[7] K. Lemmer, "Propulsion for CubeSats," *Acta Astronautica*, vol. 134, pp. 231–243, 2017.

[8] J. C. Pascoa, O. Teixeira, and G. Filipe, "A Review of Propulsion Systems for CubeSats," in *ASME International Mechanical Engineering Congress and Exposition Volume 1: Advances in Aerospace Technology*, 2018.

[9] J. Mueller, R. Hofer, and J. Ziemer, "Survey of propulsion technologies applicable to CubeSats," in *Joint Army-Navy-NASA-Air Force (JANNAF) Propulsion Meeting*, Colorado Springs, CO, 2010.

[10] D. Krejci, F. Mier-Hicks, R. Thomas, T. Haag, and P. C. Lozano, "Emission Characteristics of Passively Fed Electrospray Microthrusters with Propellant Reservoirs," *Journal of Spacecraft and Rockets*, vol. 54, no. 2, January 2017.

[11] O. Jia-Richards and P. C. Lozano, "Stage-Based Electrospray Propulsion System for Deep-Space Exploration with CubeSats," in *Proceedings of the 40th IEEE Aerospace Conference*, Big Sky, MT, March 2019.

[12] O. Jia-Richards, "Design and Analysis of a Stage-Based Electrospray Propulsion System for CubeSats," Master's thesis, Massachusetts Institute of Technology, Cambridge, MA, June 2019.

[13] D. Krejci, M. G. Jenkins, and P. C. Lozano, "Staging of electric propulsion systems: Enabling an interplanetary CubeSat," *Acta Astronautica*, vol. 160, pp. 175–182, 2019.

[14] O. Jia-Richards and P. C. Lozano, "Laboratory Demonstration of a Staging System for Electrospray Thrusters," in *Proceedings of the 36th International Electric Propulsion Conference*, Vienna, Austria, September 2019.

[15] C. Duncan and A. Smith, "Iris Deep Space CubeSat Transponder," in *Proceedings of the 11th CubeSat Workshop*, San Luis Obispo, CA, April 2014.

[16] L. P. N. Rebelo, J. N. Canongia Lopes, J. M. S. S.

Esperanca, and E. Filipe, "On the Critical Temperature, Normal Boiling Point, and Vapor Pressure of Ionic Liquids," *The Journal of Physical Chemistry B*, vol. 109, no. 13, pp. 6040–6043, 2005.

[17] C. Coffman, M. Martínez-Sánchez, F. J. Higuera, and P. C. Lozano, "Structure of the menisci of leaky dielectric liquids during electrically-assisted evaporation of ions," *Applied Physics Letters*, vol. 109, no. 23, December 2016.

[18] J. Rojas-Herrera *et al.*, "Porous Materials for Ion-Electrospray Spacecraft Microengines," *Nanomechanics and Micromechanics*, vol. 7, no. 3, September 2017.

[19] F. Mier-Hicks and P. C. Lozano, "Electrospray Thrusters as Precise Attitude Control Actuators for Small Satellites," *Journal of Guidance, Control, and Dynamics*, vol. 40, no. 3, December 2017.

[20] A. Thuppul, P. L. Wright, and R. E. Wirz, "Lifetime Considerations and Estimation for Electrospray Thrusters," in *Proceedings of 2018 Joint Propulsion Conference*, Cincinnati, OH, July 2018.

[21] P. L. Wright, A. Thuppul, and R. E. Wirz, "Life-Limiting Emission Modes for Electrospray Thrusters," in *Proceedings of 2018 Joint Propulsion Conference*, Cincinnati, OH, July 2018.

[22] N. Brikner and P. C. Lozano, "The role of upstream distal electrodes in mitigating electrochemical degradation of ionic liquid ion sources," *Applied Physics Letters*, vol. 101, no. 193504, 2012.

[23] O. Jia-Richards and P. C. Lozano, "An Analytical Framework for Staging of Space Propulsion Systems," *In Preparation*.

[24] G. J. Whiffen, "Static/dynamic control for optimizing a useful objective," United States Patent No. 6,496,741. Issued Dec. 17, 2002, Filed Mar. 25, 1999.

[25] ——, "Mystic: Implementation of the static dynamic optimal control algorithm for high-fidelity, low-thrust trajectory design," in *AIAA/AAS Astrodynamics Specialist Conference*, Keystone, CO, August 2016, Paper No. AIAA 2006-6741.

[26] A. Klesh, B. Clement, C. Colley, J. Essmiller, D. Forgette, J. Krajewski, A. Marinan, T. Martin-Mur, J. Steinkraus, D. Sternberg, T. Werne, and B. Young, "MarCO: Early Operations of the First CubeSats to Mars," in *Proceedings of the 32nd Annual AIAA/USU Conference on Small Satellites*, Logan, UT, August 2018.

[27] P. Lai, D. Sternberg, R. Haw, E. Gustafson, P. Adell, and J. Baker, "Lunar Flashlight CubeSat GNC System Development for Lunar Exploration," in *Proceedings of 2018 International Astronautical Congress*, Bremen, Germany, October 2018.

[28] J. MacArthur, B. Kristinsson, D. Freeman, E. Petro, H. Li, and P. C. Lozano, "Microfluidic and Materials Improvements in the ion Electrospray Propulsion System," in *Proceedings of the 36th International Electric Propulsion Conference*, Vienna, Austria, September 2019.

BIOGRAPHY

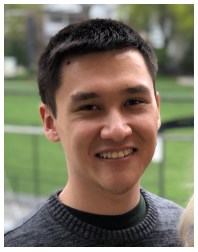

Oliver Jia-Richards *is an Sc.D. candidate and NASA Space Technology Research Fellow in the Space Propulsion Laboratory at MIT. He earned his S.B. and S.M. in aeronautical and astronautical engineering from MIT. His current research focuses on the use of electrospray thrusters for guidance and control of small spacecraft during proximity operations around small asteroids.*

David C. Sternberg *is a guidance and control systems engineer at the NASA Jet Propulsion Laboratory, having earned his S.B., S.M., and Sc.D. degrees in the MIT Department of Aeronautics and Astronautics. He is currently working on the development, testing, and operation of satellite attitude determination and control hardware for small satellites, having served as the lead attitude control system operator for the MarCO satellites, and is a guidance and control analyst for the Psyche mission.*

Daniel Grebow *is a mission design engineer in the Outer Planet Mission Analysis Group at the NASA Jet Propulsion Laboratory. He received his B.S., M.S., and Ph.D. in aeronautical and astronautical engineering from Purdue University.*

Swati Mohan *received her B.S. from Cornell University in mechanical and aerospace engineering in 2004 and earned her PhD from MIT Aero/Astro in 2010. Swati's PhD was in the MIT Space Systems Laboratory on the SPHERES project. She joined JPL in 2010 and has worked various projects since joining such as Cassini, Grail, and OCO-3. Swati is currently the lead GN&C systems engineer on the M2020 mission, specifically working on adding the terrain relative navigation system to the heritage MSL system. She is the co-founder and manager of JPL's Small Satellite Dynamics Testbed.*

Paulo C. Lozano *is the Miguel Alemán-Velasco Professor of Aeronautics and Astronautics at MIT and the director of the Space Propulsion Laboratory. He earned his S.M. and Ph.D. in space propulsion from MIT. His research features the development of highly efficient and compact ion thrusters for applications in space systems, including pico- and nano-satellites.*